The architecture of monospecific microalgae biofilms 2

Andrea Fanesi, Armelle Paule, Olivier Bernard, Romain Briandet, Filipa Lopes

microorganisms

MDPI

Article

The architecture of monospecific microalgae biofilms

Andrea Fanesi [1], Armelle Paule [1], Olivier Bernard [2], Romain Briandet[3] and Filipa Lopes[1,*]

[1] Laboratoire Génie des Procédés et Matériaux (LGPM), CentraleSupélec, Université Paris-Saclay, 91190 Gif-sur-Yvette, France
[2] Université Côte d'Azur, Inria, BIOCORE, BP 93, 06902 Sophia Antipolis Cedex, France
[3] Micalis Institute, INRA, AgroParisTech, Université Paris-Saclay, 78350 Jouy-en-Josas, France
[*] Correspondence: filipa.lopes@centralesupelec.fr; Tel.: +33175316112

Received: date; Accepted: date; Published: date

Abstract: Microalgae biofilms have been proposed as an alternative to suspended cultures in commercial and biotechnological fields. However, little is known about their architecture which may strongly impact biofilm behavior, bioprocess stability and productivity. In order to unravel the architecture of microalgae biofilms, four species of commercial interest were cultivated in microplates and characterized using a combination of confocal laser scanning microscopy and FTIR-spectroscopy. In all the species, the biofilm biovolume and thickness increased over time and reached a *plateau* after 7 days, the final biomass reached was very different though. The roughness decreased during maturation, reflecting cell division and voids filling. The extracellular polymeric substances content of the matrix remained constant in some species and increased over time in some others. Vertical profiles showed that young biofilms presented a maximum cell density at 20 µm above the substratum co-localized with matrix components. In mature biofilms, the maximum density of cells moved at a greater distance from the substratum (30-40 µm) whereas the maximum coverage of matrix components remained in deeper layer. Carbohydrates and lipids were the main macromolecules changing during biofilm maturation. Our results revealed that the architecture of microalgae biofilms is species-specific. However, time is similarly affecting the structural and biochemical parameters.

Keywords: biofilm; microalgae; architecture, confocal laser scanning microscopy, FTIR-spectroscopy

1. Introduction

In the last decades microalgae have been recognized as a valuable source of bio-products such as pigments, anti-oxidants and food supplements and they have gained popularity in a wide range of commercial activities. In conventional photobioreactors (PBRs), microalgae present low biomass concentrations (1-3 $g \cdot L^{-1}$; [1,2]) and 12 to 2000 L of liquid medium are required for the production of 1 Kg of microalgae dry mass [3]. This high water fraction requires energetic expenses for culture agitation (up to 385.71 $MJ \cdot Kg^{-1}$; [2]) and for biomass harvesting, dewatering and drying (up to 82 $MJ \cdot Kg^{-1}$; [2]). Biomass production in typical PBRs is therefore constrained by high energy and operating costs [4].

Biofilm-based cultivation systems are promising technologies overcoming the drawbacks of conventional PBRs. Such systems can reach high productivities (up to 35 g $DW \cdot m^{-2} \cdot day^{-1}$) and biomass concentration (up to 96 $g \cdot L^{-1}$; [2]). Furthermore, harvesting is simply carried out by scraping the attached biomass with minimal energy demand [3]. Finally, there is an increasing interest from the industrial sector about the great variety of molecules excreted by microalgae when developing biofilms [5]. Biofilm-based systems seem therefore to address most of the challenges of suspended cultures.

In a biofilm, microbial cells are associated with a surface and enclosed in a matrix, which is mainly composed of water, polysaccharides, proteins and nucleic acids [6]. The spatial arrangement of microorganisms and matrix components define the size and quantity of voids and channels,

altering in turn the transport of nutrients and gases [7]. The biofilm architecture induces therefore marked gradients of nutrients, gases and light along depth, inducing the cells to acclimate or displace in order to maintain an optimal growth [8,9]. Therefore, structural data are of major importance to better understand the complex behavior of biofilms (i.e. development and activity) and to improve productivity of biofilm-based technologies.

Structural changes in bacteria biofilms have been well characterized experimentally under several growth conditions, and it has been shown that the architecture is strongly species and strain dependent [10–13]. From a compositional point of view, it has been shown that changes of structural parameters in bacterial biofilms are strongly correlated to the biochemical composition of exopolymers [14–17]. Phototrophic biofilms, especially microalgae biofilms, have been far less studied [8,18–22]. In particular, little is known about the link between architecture and extracellular polymeric substances production for different species. In addition, the role played by the matrix in biofilm development has been only addressed in studies regarding mixed communities (i.e. bacteria, microalgae etc.) [8,23,24], even though microalgae are known to excrete exopolymers with specific carbohydrates:proteins:lipids:nucleic acids ratios [25,26].

In this work, we aimed therefore at better understanding how various microalgae monospecific biofilms differ in their architecture and composition depending on the species. Four biofilm-forming microalgae species of actual or potential biotechnological interest were selected, including two green algae, a red algae and a diatom. Biofilm structural dynamics and macromolecular composition were characterized by a combination of non-destructive techniques including confocal laser scanning microscopy (CLSM, which allows to characterize several structural parameters such as biovolume, thickness, roughness and diffusion distance) and vibrational spectroscopy (ATR-FTIR spectroscopy).

2. Materials and Methods

2.1. Microalgae strains and planktonic culture maintenance

Chlorella vulgaris SAG 211-11b (Göttingen, Germany) was grown in 3N-Bristol [27], the marine strain *Chlorella autothrophica* CCMP 243 (Bigelow, Maine, USA) was grown in Artificial Sea Water [28], whereas the diatom *Cylidrotheca closterium* AC170 (Caen, France) and *Porphyridium purpureum* SAG 1380-1e (Göttingen, Germany) were cultivated in filtered natural seawater. The marine media were supplemented with Walne's medium [29]; 1mL $\cdot$ L^{-1}). All biofilms were inoculated from suspended stock cultures grown in a PSI MC1000 multicultivator (Photon systems instruments, Czech Republic) in borosilicate tubes filled with 70 mL of growth medium. The cultures were bubbled and maintained semi-continuously at 25°C under a continuous photon flux density of 80 µmol photons $\cdot$ m^{-2} $\cdot$ s^{-1}. Cells from the stock cultures were harvested during the exponential phase (cell density of 2-3 $\cdot$ 10^6 cell $\cdot$ mL^{-1}).

2.2. Biofilms cultivation: inoculum, initial adhesion and growth

Biofilms were grown in polystyrene µClear ® 96-well microplates (Grenier Bio-one, France). The inoculum was prepared by diluting a volume of suspended cells (see above) to a final concentration of 1 $\cdot$ 10^6 cell $\cdot$ mL^{-1} (1 $\cdot$ 10^5 cell $\cdot$ mL^{-1} for *C. closterium*) and by transferring 250 µL of such suspension in the wells. This cell concentration corresponded to similar starting biovolume for all the species (~5 $\mu m^3 \cdot \mu m^{-2}$). The cells were then left for 24 hours adhering to the surface of the wells and subsequently 200 µL of the medium were removed in order to eliminate any unattached cell. After the first 24 hours, 80 µL of medium were removed and replaced with new medium every two days to compensate for evaporation and to buffer nutrient and CO_2 limitations. A continuous photon flux density of 100 µmol photons $\cdot$ m^{-2} $\cdot$ s^{-1} was used. Light (PAR 400-700 nm) was homogeneously provided by two sets of light emitting diode (Alpheus LED, Montgeron, France). Biofilms growth was monitored for 11 days and each day the biofilms were scanned using CLSM to detect cells signal. At day 2, 7 and 11 the biofilms were also stained to characterize the matrix and samples were harvested for ATR-FTIR spectroscopy.

2.3. Confocal laser scanning microscopy (CLSM): cells and matrix characterization

Images (512 · 512 pixels) were acquired using an inverted Zeiss LSM700 confocal microscope (Carl Zeiss microscopy GmbH, Germany) controlled using the Zen 10.0 software black edition (Carl Zeiss microscopy GmbH, Germany). All biofilms were scanned with a LD Plan-Neofluar 20x/0.4 Korr M27 objective with a 0.4 N.A. (numerical aperture). Each image was 638 · 638 μm in size with a z-step of 3.94 μm. The settings of the confocal microscope are reported in Table S1. After preliminary trials, a low magnification lens was preferred to a higher one (e.g. 63x), because allowing to scan wider biofilm areas (essential to properly capture microalgae cell patterns) and to acquire z-stacks over the whole biofilm depth. However, we have to point out that this choice comes with side effects, such as a greater point spread function and a lower resolution of the images.

Two laser lines were used to respectively detect microalgae and the matrix surrounding them. Microalgae cells were observed by detecting chlorophyll *a* auto-fluorescence. Lectins and dextran (3kDa), both labelled with fluorescein (FITC), were added at day 2, 7 and 11 to detect glycoconjugates and to visualize non-specifically the matrix, respectively [30–33]. The pool of extracellular glycoconjugates (i.e. exopolysaccharides, glycoproteins etc.) specifically detected by the lectins will be identified here as EPS (extracellular polymeric substances). Dextran on the other hand is supposed to diffuse into the channels, voids and to get finally non-specifically trapped into the matrix [30–33]. A fresh cocktail of 20 lectins (Kit I, II and III, Vector Laboratories, Peterborough, UK) or dextran were supplied at a final concentration of 13 $\mu g \cdot mL^{-1}$. The microplates were then incubated in the dark for 30 minutes. Afterwards, the excess of dyes present in the wells was removed by carefully removing 140 μL of the medium and by adding other 140 μL of fresh medium (specific for each species) in each well. This process was repeated one time for the dextran and two times for the lectins. We have to point out that since a mixture of lectins was used to detect the matrix, it is possible that the interaction among the single lectins and the competition for similar targets may have occurred.

Chlorophyll *a* was excited with the 639 nm line of a 5 mW solid state diode laser and the emission of chlorophyll *a* auto-fluorescence was observed using the long pass (LP) filter 615 nm. Lectins and dextran were excited with the 488 nm laser line of a 10 mW solid state diode laser and their fluorescence detected using the band pass (BP) filter 490-530 nm. Unlabeled organisms and wells filled with growth media but not inoculated with microalgae were used as a staining control. Each well was scanned on at least three random positions (three z-stacks) resulting in a total surface area of at least 1.2 mm^2.

2.4. Image analysis

The plug-in COMSTAT 2.1 (Technical University of Denmark; [11]) running in ImageJ 1.48v [34] was used to extract from the images the quantitative parameters typically used to characterize biofilm structures. The complete list of parameters is reported in Table S2. Images binarization was automatically computed in the plug-in by selecting a threshold value using the Otsu algorithm [35] and the function "connected volume filtering" was unchecked.

Since the auto-fluorescence of the cells comes from the chlorophyll within the chloroplasts, we have to point out that the structural parameter calculated from the images reflect such organelle rather than the whole cell, even though the overlapping of fluorescence and transmission images revealed good matching of the two acquisition mode (data not shown). However, to be consistent with the terminology present in most of the literature, we considered that the auto-fluorescence of the chlorophyll quantifies the cells.

2.5. ATR-FTIR spectroscopy

At day 2, 7 and 11, the biofilms were scrapped from four wells for each species. The samples were centrifuged at 8000 · *g* for 5 minutes and the supernatant removed. After that, 1 mL of distilled water in the case of *C. vulgaris* and 1 mL of a solution of NaCl (35 $g \cdot L^{-1}$) for the marine species were used to wash the biofilm suspensions from salts that would otherwise interfere with the cell and

matrix spectral signature. Afterward, the pellet was re-suspended in 5-10 μL of distilled water or NaCl and 1.5 μL were transferred on a 45° ZeSe flat crystal of an ATR-FTIR PerkinElmer Spectrum-two spectrometer (PerkinElmer, Waltham, USA) and the sample was dried at room temperature for 20 minutes. Spectra were acquired in the range 4000 and 400 cm^{-1} using 32 accumulations at a spectral resolution of 4 cm^{-1}. Before each measurement, the empty crystal was measured using the same instrumental setting and used as a blank.

Spectra were baselined using the rubberband algorithm and the ratios between the main macromolecular pool (proteins, lipids and carbohydrates) were calculated as the ratios between the maximum absorption values for the spectral ranges corresponding to each macromolecular pool: proteins (Amide I; 1700-1630 cm^{-1}), lipids (C=O; 1750-1700 cm^{-1}) and carbohydrates (C-O-C, C-C and Si-O-Si in diatoms; 1200-950 cm^{-1}). Since no separation between cells and matrix components was performed, the spectra reflected both the physiological changes occurring in the cells and those related to EPS.

2.6. Statistics

Statistics was performed using GraphPad prism 5.0 (San Diego, CA, USA) and R [36]. One-way and two-way ANOVA were used to test the statistical significance of mean differences among different species and over time. The level of significance was always set at 5%. The logistic function [37,38] was fit to the biovolume vs. time curves and the maximal cell biovolume (i.e. the biovolume at the *plateau*) and the specific growth rate (μ) were obtained in order to make quantitative comparisons between the species.

Correlation matrices, using the Pearson's coefficient, were computed using the package "corrplot" [39] present in R to investigate the relationship among structural parameters (obtained from CLSM) and biofilms macromolecular composition (FTIR ratios).

All results are reported as mean and standard deviations of several independent biological replicates. Biofilm dynamics were repeated on at least four independent microplates. In each microplate, for each species and for each time point, at least three separate wells were analyzed by CLSM. In each well, at least three randomly chosen biofilm areas were scanned.

3. Results

3.1. Biofilm development over time: structural characteristics

Examples of 3D biofilm reconstructions are reported in Figure 1a. The biovolume of the cells within the biofilm increased over time and after seven days the *plateau* was reached for all the species (Figure 2a). *C. autotrophica* and *P. purpureum* exhibited the highest biovolume, whereas *C. vulgaris* and *C. closterium* presented almost 50% lower biovolume. *C. autotrophica* also exhibited the highest growth rate whereas no significant difference was found among the other microalgae (Table 1 and Figure 2a; $p > 0.05$).

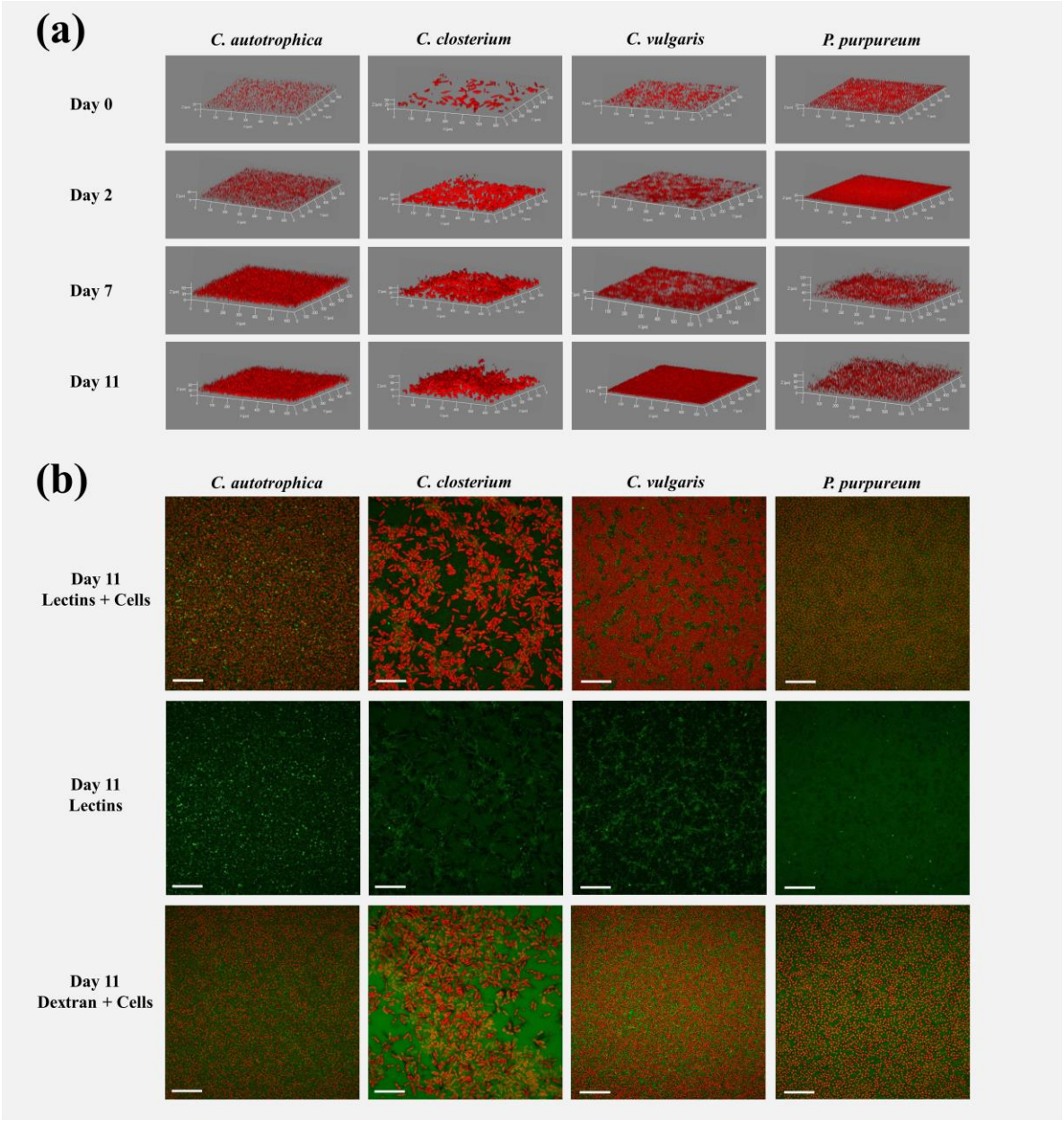

Figure 1. Representative three-dimensional reconstructions of the microalgae biofilms (a) and maximum intensity projection (b) of cells (red signal), lectins (green signal) and dextran (green signal) signals of the biofilms at day 11. In panel (a), day 0 represents the inoculum, day 2, 7 and 11 are the days at which the biofilms were stained and analyzed by ATR-FTIR spectroscopy. The brightness of the images was adjusted for better visualization. Images size in (a) and (b) is 638 · 638 μm. The XY ticks interval in (a) is 100 μm and the scale bar in (b) is 100 μm.

197 **Table 1.** Growth parameters (growth rate and maximal biovolume) obtained by fitting the logistic
198 regression to the biovolume vs. time curves. Data are reported as the mean and standard deviation of at least
199 nine independent biological replicates. Different letters represent statistically different means (p<0.05) as
200 determined by pair-wise comparisons after one-way ANOVA.

Microalgae species	**μ (d^{-1})**	**Maximal biovolume ($\mu m^3 \cdot \mu m^{-2}$)**
C. autotrophica	0.72^{a} (0.24)	50.47^{a} (4.09)
C. vulgaris	0.45^{b} (0.14)	31.22^{c} (8.49)
P. purpureum	0.65^{ab} (0.20)	43.02^{b} (4.92)
C. closterium	0.43^{b} (0.13)	22.42^{d} (2.59)

201
202 Roughness presented an opposite trend to biovolume and decreased (from 1.2 to 0.2 a.u.) over
203 time in *C. autotrophica*, *C. vulgaris* and *P. purpureum*. The roughness coefficient of *C. closterium* instead,
204 remained stable at values around one (Figure 2b).
205 Over time, the increase in biomass resulted in a thickening of the biofilms (Figure 2c,d). *C.*
206 *autotrophica* developed the thickest biofilms (~100 μm) and its maximum thickness remained stable
207 over time. *P. purpureum* and *C. closterium* presented a similar increase of the maximum thickness
208 reaching values like those of *C. autotrophica*. *C. vulgaris* presented thinner biofilms with a maximum
209 thickness around 30-40 μm. The average thickness of *C. autotrophica* increased rapidly during the first
210 four days and then levelled off around 80 μm at day 7. *P. purpureum*, *C. closterium* and *C. vulgaris*
211 exhibited a more linear increase of the average thickness. *P. purpureum* reached a similar thickness to
212 that of *C. autotrophica* whereas *C. closterium* and *C. vulgaris* at the end presented 40-50% lower
213 thicknesses with respect to *C. autotrophica*.
214 The maximum diffusion distance increased over time in all the species but *C. vulgaris* (Figure
215 2e). At the end of the assay *C. autotrophica* and *C. closterium* presented similar values and reached the
216 highest values among all species, followed by *P. purpureum* and *C. vulgaris*. The average diffusion
217 distance followed a similar pattern to biovolume: it increased rapidly the first four days and then
218 leveled off from day 7 (Figure 2f). *C. autotrophica*, *C. vulgaris* and *P. purpureum* presented comparable
219 average diffusion distance (0.6-0.9 μm) whereas *C. closterium* exhibited the lowest (0.1-0.3 μm; p<0.05).

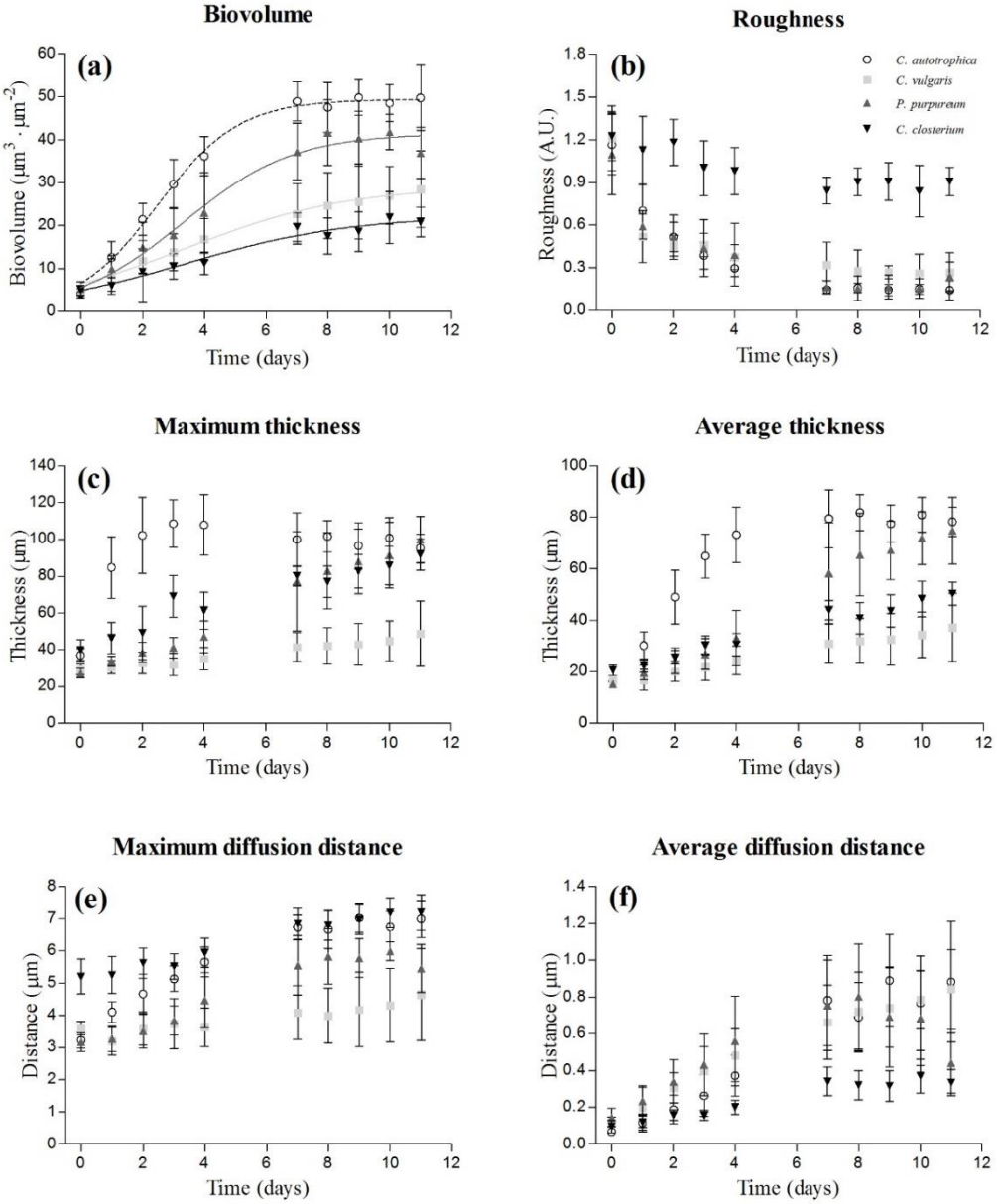

Figure 2. Dynamics of the structural parameters obtained from the z-stacks acquired at the CLSM: biovolume (a), roughness (b), maximum thickness (c), average thickness (d), maximum diffusion distance (e) and average diffusion distance (f). The results are reported as the mean and standard deviation of 12 independent biological replicates. The fitting of the logistic model is also presented for the biovolume.

3.2. Matrix characterization: lectins and dextran volumes

In order to characterize the matrix of the biofilms, the volume of binding lectins and of dextran was quantified. The volume of lectins reflected the fraction of glycoconjugates (EPS) in the matrix and dextran was used to quantify voids, water channels and non-specifically the whole matrix (Figure 1b).

C. vulgaris presented the lowest amount of EPS (Figure 3a), whereas it increased over time in *P. purpureum* and *C. closterium* biofilms, which volume of EPS doubled from day 2 to day 7. No temporal change was observed for *C. autotrophica* and *C. vulgaris* (p>0.05). *C. closterium* presented the highest lectins to cells ratio (Figure 3b). Over time, *C. autotrophica* exhibited a decrease over time in the lectins to cells ratio (p<0.05) whereas in the other species the ratio remained stable.

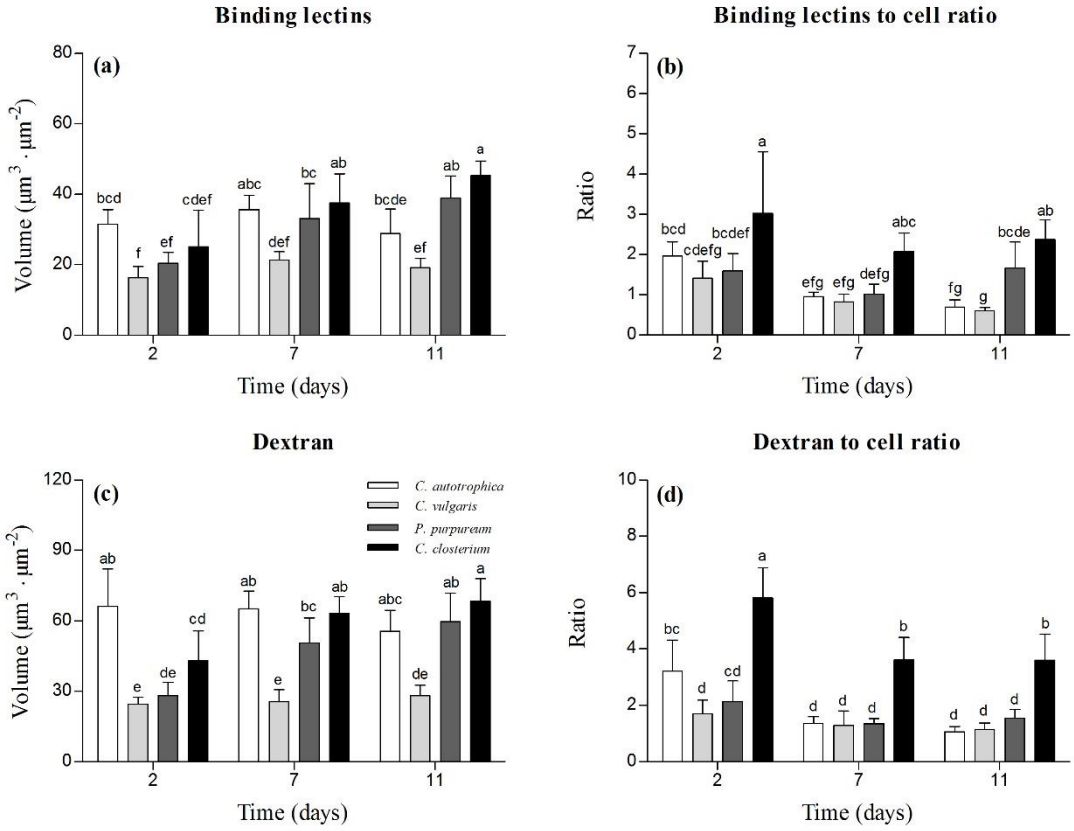

Figure 3. Structural parameters characterizing the biofilm matrix at day 2, 7 and 11. Volume of binding lectins ((a); specifically binding to glycoconjugates), lectins to cells ratio (b), volume of dextran ((c); used to stain non-specifically the matrix), and dextran to cell ratio (d). The results are reported as the mean and standard deviation of at least four independent biological replicates. Bars with different letters represent statistically different means (p<0.05) as determined by pair-wise comparisons after two-way ANOVA.

At day 2, the volume of dextran was the highest in *C. autotrophica* biofilms (~65 μm³ · μm⁻²). *P. purpureum* and *C. closterium* presented 50% and 30% lower volume of dextran in their matrix, but at day 7 and 11, they approached the values of *C. autotrophica* (Figure 3c). *C. vulgaris* always presented the lowest volume of dextran in the matrix (~30 μm³ · μm⁻²). In *C. autotrophica* and *C. vulgaris*, no significant change was observed over time (Figure 3c). Similarly to lectins, the dextran to cells ratio was always the highest in *C. closterium* and it decreased from day 2 to 7 and then levelled off. A similar ratio was found for *C. autotrophica C. vulgaris* and *P. purpureum*. *C. autotrophica* presented a decreasing trend from day 2 to day 7 similar to *C. closterium*. *C. vulgaris* and *P. purpureum* biofilms did not show any significant change over time of the dextran to cells ratio (Figure 3d).

3.3. Areal coverage over depth: cells vs. matrix vertical profiles

Regardless of the species, the maximum of cell density was reached at day 2, at a distance from the substratum of 10 μm, where the cells were already covering almost 50% of the area, except for *C. closterium* that only covered 30% of the area (Figure 4g). On the other hand, during maturation, the maximal percentage of cell coverage moved at a greater distance (30-40 μm) above the substratum and the depth at which it was reached and the percentage of coverage were species-specific (ranging from 40 to 90% of covered area; Figure 4).

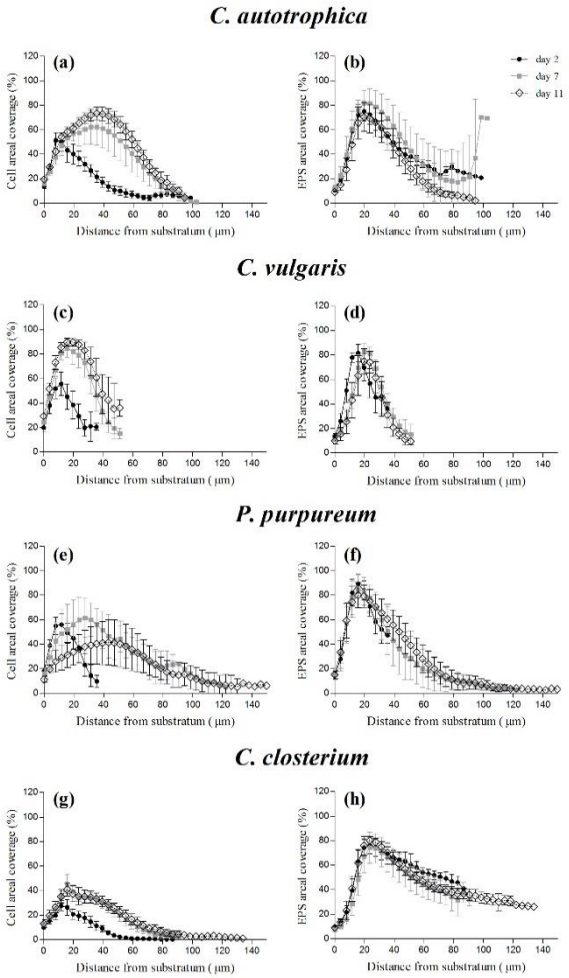

Figure 4. Vertical profiles of cells (a, c, e, g) and EPS (b, d, f, h) coverage of four different monospecific microalgae biofilms after 2, 7 and 11 days of maturation. The vertical profiles are reported as the percentage of coverage of cells or of EPS obtained from the z-stacks acquired at the CLSM. The vertical profiles are reported as the mean and standard deviation of at least four independent biological replicates.

Dextran and lectins presented comparable distributions over depth (Figure 4b,d,f,h and Figure S1). Interestingly, although the cells profile over depth changed as a function of time, the highest density of EPS and voids seemed to be positioned close to the substratum (20-30 μm) at all time points and for all the species.

In addition, the depth of maximum cells density presented a positive correlation with the average biofilm thickness (R^2 = 0.78, p=0.0001). On the other hand, for the EPS the regression slope was not significantly different from zero (Figure S2; R^2 = 0.005, p=0.81).

3.4. Biofilm biochemical characterization by ATR-FTIR spectroscopy and correlation analysis with structural data

The average FTIR spectra of the biofilms at the different sampling times (day 2, 7 and 11) are reported in Figure S3. *C. autotrophica* and *P. purpureum* were the species that presented the greatest macromolecular changes along time.

Similar carbohydrates to proteins ratios were observed for all the samples and the ratio did not change in *C. vulgaris*, *C. closterium* and *C. autotrophica* (Figure 5a; p>0.05). In contrast for *P. purpureum*, the carbohydrates to proteins ratio was 50% higher at day 11 than that at day 2 (Figure 5a; p<0.05). *P. purpureum* and *C. vulgaris* biofilms did not exhibit any change in the lipids to proteins ratio (Figure

5b; $p>0.05$). For *C. autotrophica* biofilms, the lipids to proteins ratio increased by 50% at day 11 compared to day 2 (Figure 5b; $p<0.05$) and for *C. closterium* it increased by 30% at day 7 compared to day 2.

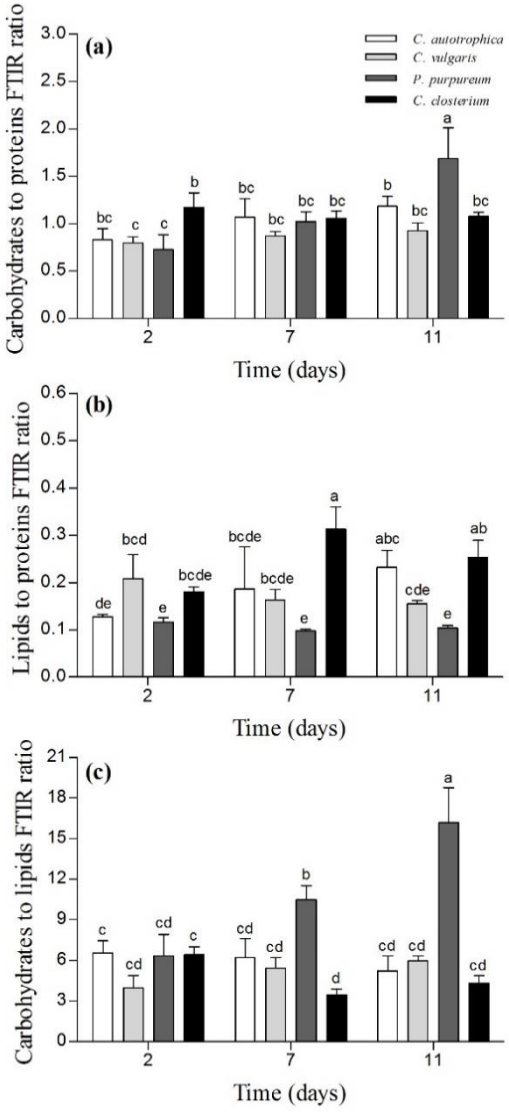

Figure 5. Macromolecular composition of the biofilms after 2, 7 and 11 days of maturation. The panel (a) depicts the carbohydrates to proteins ratio, the panel (b) depicts the lipids to proteins to ratio and the panel (c) represents the carbohydrates to lipids ratio. The results are reported as the mean and standard deviation of at least four independent biological replicates. Bars with different letters represent statistically different means ($p<0.05$) as determined by pair-wise comparisons after the two-way ANOVA.

In *C. autotrophica* and *C. vulgaris* biofilms, the carbohydrates to lipids ratio did not change over time ($p>0.05$). For *P. purpureum* it tripled between day 2 and day 11. In *C. closterium*, the ratio was lower at day 7 compared to day 2 (almost 50%), but no difference was found between day 11 and day 2 (Figure 5c).

A correlation analysis was carried out to identify the possible correlations among the macromolecular ratios and the matrix of structural data (Figure S4). In *P. purpureum*, the EPS and dextran volumes were positively correlated to the carbohydrates to proteins and to the carbohydrates to lipids ratios whereas they were negatively correlated to the lipids to proteins ratio. In all the other

299 species, only minor correlations were found between matrix components and the macromolecular
300 pools (Figure S4). In contrast, for these species the macromolecular ratios were correlated to the
301 structural parameters obtained from cells autofluorescence such as thickness, biovolume, diffusion
302 distance and roughness (Figure S4).

303 **4. Discussion**

304 Our results show that the architecture of microalgae biofilms is species dependent. But the
305 structure evolution over time seemed to follow some general common rules that resemble those
306 described for bacteria and fungi [11,40–42].
307 During the first stages of substrate colonization the biofilms were irregular in their surfaces (i.e.
308 high roughness), thin and for some of the species the volume of EPS was higher than that of the cells
309 (Figure 2 and 3). As the biofilms matured, the biovolume increased reflecting active cell division,
310 similarly to what was reported for phototrophic biofilms by Mueller et al. [8] and Kernan et al. [20].
311 Mueller et al. [8] reported a linear increase whereas our growth curves and those from Kernan et al.
312 [20] reached a *plateau* (Figure 2a). Mueller et al. [8] focused on a natural mixed community including
313 bacteria and different species of microalgae. Therefore, the species succession over time with different
314 physiological requirements may have led to a continuous growth. In our case and for Kernan et al.
315 [20], the biofilms were composed by a single species that may have experienced over time energy or
316 nutrients limitation leading to a slowdown of the growth. Since nutrients were replenished every two
317 days, light was probably the limiting factor. Barranguet et al. [23] reported for instance that light was
318 attenuated up to 90% in mature phototrophic biofilms [23], whereas Schnurr et al. [43] reported that
319 the transmitted light for a biofilm with a thickness of 100 μm (similar to the ones reported in this
320 study) was only 12% of the incident light. This means that for a photon flux density of 100 μmol · m^{-2} · s^{-1} the cells in the deeper layers of the biofilm would receive only 12 μmol · m^{-2} · s^{-1}, an intensity far
322 below the light compensation point measured for example in *C. vulgaris* biofilm (30-60 μmol photons
323 · m^{-2} · s^{-1}; [44]).
324 The roughness of the biofilms decreased over time along with the progressive filling of the initial
325 voids by new daughter cells (Figure 2b). A similar behavior has been described for natural multi-
326 specific river biofilms [45] and for bacteria biofilms [10,41]. Mueller et al. [8] on the other hand,
327 reported a positive correlation between biovolume and roughness and a parallel increase of diatoms
328 over time. This is in agreement with the biofilm of the diatom *C. closterium* that exhibited only minor
329 changes of roughness over time (Figure 2b). The progression from rough to smoother surfaces as a
330 biofilm mature has been proposed to be dependent either on cells metabolic rate or on the maximum
331 internal transport rate of nutrients [46,47]. In the case of cells with low metabolic activity (and
332 therefore high nutrient availability) the valley between the biofilm peaks grow and merge with
333 adjacent peaks decreasing the roughness of a biofilm. Cells with high metabolic rate might become
334 nutrient limited and division will proceeds only at the biofilm peaks (i.e. along the vertical nutrient
335 gradients; [46,47]), inducing the formation of finger-like structures. Based on these observations, the
336 development of smoother biofilms along time, in *P. purpureum*, *C. vulgaris* and *C. autotrophica*, as
337 compared to the rougher structured biofilms in *C. closterium*, may reflect different cell metabolic rates.
338 Further metabolic investigations, such as intracellular measurements or O_2 evolution, will be
339 necessary to validate these conclusions.
340 As the majority of studies on photosynthetic biofilms focused on natural mixed communities
341 (i.e. formed by bacteria and microalgae), little is known about EPS dynamics in microalgae biofilms.
342 Here, we report the ability of microalgae to set up a supporting matrix and the dynamics of EPS
343 during biofilm development. Interestingly, whereas the dynamics of cells were similar among all the
344 species (Figure 2), those of EPS were more species-specific (Figure 3a): the two green algae did not
345 show any quantitative change of the EPS whereas *P. purpureum* and *C. closterium* presented a greater
346 volume of EPS over time. These different trends are in agreement with the great variety of dynamics
347 reported elsewhere as a function of the community composition. Trends of EPS production in
348 photosynthetic biofilms present in the literature are indeed very disparate [8,23,24]. Ratios of matrix
349 components (either considering lectins or dextran) to cells were not significantly different over time

for all species, which may indicate a stable physiological state of the cells within the biofilm. Interestingly, they were positively correlated to the biofilm roughness coefficient, indicating that irregular surfaces were associated with high EPS content and low cell biovolume. Similar ratios of EPS to cells have been reported for stream mixed biofilms by Battin et al. [45], which proposed that high EPS content may be advantageous for the attachment of the cells and first colonization of the substratum.

During biofilm development, several processes such as cell growth, EPS excretion or consumption [48], as well as the establishment of chemical and physical gradients may be responsible for the vertical distribution of cells and matrix components [9]. The few literature data about z-profiles in photosynthetic biofilms indicate that the distribution of cells and EPS is very much dependent on the culture conditions and on the biofilm nature (bacteria, algae or mixed communities), nevertheless some patterns can be drawn [8,18,20,23]. The maximal coverage for photosynthetic organisms seems to occur within the first 40 μm from the substratum, whereas EPS seem to match the cells position in young biofilms and to be mostly placed in layers above the cells in older biofilms. In our work, at day 2 the cell z-profile was consistent with the patterns described in the literature: maximal areal coverage of the cells positioned at 20 μm from the substratum (Figure 4) and greatest coverage of EPS typically co-localized with the cells in proximity of the substratum (~20 μm). This means that the matrix components were mostly interspersed between the cells [49]. Along time, the maximal areal coverage of the cells moved at greater distances from the substratum as described in Cole et al. [18] but the location of the maximum EPS density remained stable over time (Figure 4). It is therefore likely that the production of EPS in deep layers may have been responsible for the upward growth of the biofilm by global advection [48,50] This is also supported by the fact that the maximum cell coverage moved upward as a function of the biofilm thickness whereas the EPS maximal coverage remained stable (Figure S2).

In bacteria, changes in biofilms structures have been reported to be strongly related to qualitative shift in the macromolecular composition of the EPS, which in turn may alter biofilms functions and properties [14,15,17,51]. In order to evaluate the relationships among macromolecules and structures in microalgae biofilms, a correlation analysis using the CLSM and FTIR results was performed. Lipids and/or carbohydrates changed in concentration as the biofilms matured and their architecture became more complex (Figure 5 and S3). The lack of correlation between the macromolecular changes and the EPS and dextran volumes (except for *P. purpureum*) might indicate a reallocation of carbon in the cells rather than changes in matrix components. *P. purpureum* behaved differently, and such changes were positively correlated to the EPS and dextran volumes (Figure S4), suggesting an increase in glycoconjugates in the matrix as the biofilm matured [52].

Concluding, the development, architecture and macromolecular composition of monospecific microalgae biofilms seem to be strongly species-dependent. The selection of a microalgae strain for further cultivation in biofilm-based systems is therefore a crucial step for the whole process as specific structural features maybe more or less advantageous under a certain set of culture conditions. Future studies will be required to address how hydrodynamics and the fluctuating light conditions, characteristic of outdoor cultivation systems, influence the structures and composition of algal biofilms. The data recorded in this study may be used to feed and calibrate photosynthetic growth models to better understand the mechanisms behind biofilm development under different conditions [53]. Extension of these models for large-scale production can be used for optimal process design or to guide the process operations. Furthermore, microfluidic tools or larger flow-cells are promising tools for completing the picture and eventually providing an overview of the advantages and pitfalls of using microalgae biofilm-based system [22]

Supplementary Materials: The following are available online at www.mdpi.com/xxx/s1, Figure S1: Vertical profiles of cells and dextran, Figure S2: Dependency of the depth of maximal coverage of cells and glycoconjugates (EPS) as a function of the average biofilm thickness, Figure S3: ATR-FTIR spectra of microalgae biofilms, Figure S4: Correlation plot, Table S1: Instrumental settings of the confocal microscope, Table S2: Biofilm structural parameters calculated using COMSTAT 2.1.

Author Contributions: Conceptualization, Andrea Fanesi, Armelle Paule, Olivier Bernard, Romain Briandet and Filipa Lopes; Data curation, Andrea Fanesi and Armelle Paule; Formal analysis, Andrea Fanesi and Armelle Paule; Funding acquisition, Olivier Bernard, Romain Briandet and Filipa Lopes; Methodology, Andrea Fanesi and Armelle Paule; Supervision, Olivier Bernard, Romain Briandet and Filipa Lopes; Writing – original draft, Andrea Fanesi and Armelle Paule; Writing – review & editing, Andrea Fanesi, Olivier Bernard, Romain Briandet and Filipa Lopes.

Funding: This work has benefited from the financial support of the LabeX LaSIPS project AlgaeBiofilm and Greenbelt managed by the French National Research Agency (ANR).

Acknowledgments: The authors acknowledge Cyril Breton and Thierry Martin for the technical support regarding confocal microscopy, image analysis and light systems.

Conflicts of Interest: The authors declare no conflict of interest. The funders had no role in the design of the study; in the collection, analyses, or interpretation of data; in the writing of the manuscript, or in the decision to publish the results.

References

1. Jorquera, O.; Kiperstok, A.; Sales, E.A.; Embiruçu, M.; Ghirardi, M.L. Comparative energy life-cycle analyses of microalgal biomass production in open ponds and photobioreactors. *Bioresour. Technol.* **2010**, *101*, 1406–1413.
2. Ozkan, A.; Kinney, K.; Katz, L.; Berberoglu, H. Reduction of water and energy requirement of algae cultivation using an algae biofilm photobioreactor. *Bioresour. Technol.* **2012**, *114*, 542–548.
3. Berner, F.; Heimann, K.; Sheehan, M. Microalgal biofilms for biomass production. *J. Appl. Phycol.* **2015**, *27*, 1793–1804.
4. Slade, R.; Bauen, A. Micro-algae cultivation for biofuels: Cost, energy balance, environmental impacts and future prospects. *Biomass and Bioenerg.* **2013**, *53*, 29–38.
5. Di Pippo, F.; Ellwood, N.T.W.; Gismondi, A.; Bruno, L.; Rossi, F.; Magni, P.; De Philippis, R. Characterization of exopolysaccharides produced by seven biofilm-forming cyanobacterial strains for biotechnological applications. *J. Appl. Phycol.* **2013**, *25*, 1697–1708.
6. Sutherland, I.W. The biofilm matrix – an immobilized but dynamic microbial environment. *Trends Microbiol.* **2001**, *9*, 222–227.
7. Beer, D. de; Stoodley, P.; Roe, F.; Lewandowski, Z. Effects of biofilm structures on oxygen distribution and mass transport. *Biotechnol. Bioeng.* **1994**, *43*, 1131–1138.
8. Mueller, L.N.; de Brouwer, J.F.; Almeida, J.S.; Stal, L.J.; Xavier, J.B. Analysis of a marine phototrophic biofilm by confocal laser scanning microscopy using the new image quantification software PHLIP. *BMC Ecol.* **2006**, *6*, 1.
9. Stewart, P.S.; Franklin, M.J. Physiological heterogeneity in biofilms. *Nat. Rev. Microbiol.* **2008**, *6*, 199–210.
10. Bridier, A.; Dubois-Brissonnet, F.; Boubetra, A.; Thomas, V.; Briandet, R. The biofilm architecture of sixty opportunistic pathogens deciphered using a high throughput CLSM method. *J. Microbiol. Methods* **2010**, *82*, 64–70.
11. Heydorn, A.; Nielsen, A.T.; Hentzer, M.; Sternberg, C.; Givskov, M.; Ersbøll, B.K.; Molin, S. Quantification of biofilm structures by the novel computer program COMSTAT. *Microbiology* **2000**, *146*, 2395–2407.
12. Srinandan, C.S.; Jadav, V.; Cecilia, D.; Nerurkar, A.S. Nutrients determine the spatial architecture of *Paracoccus sp.* biofilm. *Biofouling* **2010**, *26*, 449–459.
13. Staudt, C.; Horn, H.; Hempel, D.C.; Neu, T.R. Volumetric measurements of bacterial cells and extracellular polymeric substance glycoconjugates in biofilms. *Biotechnol. Bioeng.* **2004**, *88*, 585–592.

14. Desmond, P.; Best, J.P.; Morgenroth, E.; Derlon, N. Linking composition of extracellular polymeric substances (EPS) to the physical structure and hydraulic resistance of membrane biofilms. *Water Res.* **2018**, *132*, 211–221.
15. Garny, K.; Neu, T.R.; Horn, H.; Volke, F.; Manz, B. Combined application of 13C NMR spectroscopy and confocal laser scanning microscopy—Investigation on biofilm structure and physico-chemical properties. *Chem. Eng. Sci.* **2010**, *65*, 4691–4700.
16. Kawaguchi, T.; Decho, A.W. Biochemical characterization of cyanobacterial extracellular polymers (EPS) from modern marine stromatolites (Bahamas). *Prep. Biochem. Biotechnol.* **2000**, *30*, 321–330.
17. Tan, L.; Zhao, F.; Han, Q.; Zhao, A.; Malakar, P.K.; Liu, H.; Pan, Y.; Zhao, Y. High correlation between structure development and chemical variation during biofilm formation by *Vibrio parahaemolyticus*. *Front. Microbiol.* **2018**, *9*.
18. Cole, J.K.; Hutchison, J.R.; Renslow, R.S.; Kim, Y.-M.; Chrisler, W.B.; Engelmann, H.E.; Dohnalkova, A.C.; Hu, D.; Metz, T.O.; Fredrickson, J.K.; et al. Phototrophic biofilm assembly in microbial-mat-derived unicyanobacterial consortia: model systems for the study of autotroph-heterotroph interactions. *Front. Microbiol.* **2014**, *5*.
19. David, C.; Bühler, K.; Schmid, A. Stabilization of single species *Synechocystis* biofilms by cultivation under segmented flow. *J Ind Microbiol Biotechnol* **2015**, *42*, 1083–1089.
20. Kernan, C.; Chow, P.P.; Christianson, R.J.; Huang, J. Experimental and computational investigation of biofilm formation by *Rhodopseudomonas palustris* growth under Two Metabolic Modes. *PLOS ONE* **2015**, *10*, e0129354.
21. Norcy, T.L.; Niemann, H.; Proksch, P.; Linossier, I.; Vallée-Réhel, K.; Hellio, C.; Faÿ, F. Anti-biofilm effect of biodegradable coatings based on Hemibastadin derivative in marine environment. *Int. J. Mol. Sci.* **2017**, *18*, 1520.
22. Le Norcy, T.; Faÿ, F.; Obando, C.Z.; Hellio, C.; Réhel, K.; Linossier, I. A new method for evaluation of antifouling activity of molecules against microalgal biofilms using confocal laser scanning microscopy-microfluidic flow-cells. *Int. Biodet. Biodegr.* **2019**, *139*, 54–61.
23. Barranguet, C.; Beusekom, S.A.M. van; Veuger, B.; Neu, T.R.; Manders, E.M.M.; Sinke, J.J.; Admiraal, W. Studying undisturbed autotrophic biofilms: still a technical challenge. *Aquat. Microb. Ecol.* **2004**, *34*, 1–9.
24. Neu, T.R.; Swerhone, G.D.W.; Böckelmann, U.; Lawrence, J.R. Effect of CNP on composition and structure of lotic biofilms as detected with lectin-specific glycoconjugates. *Aquat. Microb. Ecol.* **2005**, *38*, 283–294.
25. de Jesus Raposo, M.F.; de Morais, A.M.M.B.; de Morais, R.M.S.C. Bioactivity and applications of polysaccharides from marine microalgae. In *Polysaccharides: Bioactivity and Biotechnology*; Ramawat, K.G., Mérillon, J.-M., Eds.; Springer International Publishing: Cham, **2015**; pp. 1683–1727 ISBN 978-3-319-16298-0.
26. Xiao, R.; Zheng, Y. Overview of microalgal extracellular polymeric substances (EPS) and their applications. *Biotechnol. Adv.* **2016**, *34*, 1225–1244.
27. Bischoff, H.W.; Bold, H.C. Phycological Studies IV. Some soil algae from enchanted rock and related algal species. *University of Texas publication* **1963**, *6318*, 95.
28. Lyman, J.; Fleming, R.H. Composition of sea water. *J. Mar. Res.* **1940**, 134–146.
29. Walne, P.R. Studies on the food value of nineteen genera of algae to juvenile bivalves of the genera *Ostrea*, *Crassostrea*, *Mercenaria* and *Mytilus*. *Fish. Invest. Ser.* **1970**, *2 26*.
30. Assaf, D.; Steinberg, D.; Shemesh, M. Lactose triggers biofilm formation by *Streptococcus mutans*. *Int. Dairy J.* **2015**, *42*, 51–57.

31. Klein, M.I.; Duarte, S.; Xiao, J.; Mitra, S.; Foster, T.H.; Koo, H. Structural and molecular basis of the role of starch and sucrose in *Streptococcus mutans* biofilm development. *Appl. Environ. Microbiol.* **2009**, *75*, 837–841.
32. Koo, H.; Xiao, J.; Klein, M.I.; Jeon, J.G. Exopolysaccharides produced by *Streptococcus mutans* glucosyltransferases modulate the establishment of microcolonies within multispecies biofilms. *J. Bacteriol.* **2010**, *192*, 3024–3032.
33. Lawrence, J.R.; Wolfaardt, G.M.; Korber, D.R. Determination of diffusion coefficients in biofilms by Confocal Laser Microscopy. *Appl. Environ. Microbiol.* **1994**, *60*, 1166–1173.
34. Schneider, C.A.; Rasband, W.S.; Eliceiri, K.W. NIH Image to ImageJ: 25 years of image analysis. *Nat. Methods* **2012**, *9*, 671–675.
35. Otsu, N. A treshold selection method from gray-level histograms. 5.
36. R Core Team R: A language and environment for statistical computing. **2014**, Foundation for Statistical Computing, Vienna, Austria. URL http://www.R-project.org/.
37. Tsai, Y.-P. Impact of flow velocity on the dynamic behaviour of biofilm bacteria. *Biofouling* **2005**, *21*, 267–277.
38. Wang, C.; Miao, L.; Hou, J.; Wang, P.; Qian, J.; Dai, S. The effect of flow velocity on the distribution and composition of extracellular polymeric substances in biofilms and the detachment mechanism of biofilms. *Water Sci. Technol.* **2014**, *69*, 825–832.
39. Wei, T.; Simko, V. R package "corrplot": Visualization of a correlation matrix (Version 0.84). **2017**, Available from https://github.com/taiyun/corrplot.
40. Kolderman, E.; Bettampadi, D.; Samarian, D.; Dowd, S.E.; Foxman, B.; Jakubovics, N.S.; Rickard, A.H. L-Arginine destabilizes oral multi-species biofilm communities developed in human saliva. *PLOS ONE* **2015**, *10*, e0121835.
41. Li, L.; Jeon, Y.; Lee, S.-H.; Ryu, H.; Santo Domingo, J.W.; Seo, Y. Dynamics of the physiochemical and community structures of biofilms under the influence of algal organic matter and humic substances. *Water Res.* **2019**, *158*, 136–145.
42. Seneviratne, C.J.; Silva, W.J.; Jin, L.J.; Samaranayake, Y.H.; Samaranayake, L.P. Architectural analysis, viability assessment and growth kinetics of *Candida albicans* and *Candida glabrata* biofilms. *Arch. Oral Biol.* **2009**, *54*, 1052–1060.
43. Schnurr, P.J.; Espie, G.S.; Allen, D.G. The effect of light direction and suspended cell concentrations on algal biofilm growth rates. *Appl. Microbiol. Biotechnol.* **2014**, *98*, 8553–8562.
44. Rincon, S.M.; Urrego, N.F.; Avila, K.J.; Romero, H.M.; Beyenal, H. Photosynthetic activity assessment in mixotrophically cultured *Chlorella vulgaris* biofilms at various developmental stages. *Algal Res.* **2019**, *38*, 101408.
45. Battin, T.J.; Kaplan, L.A.; Newbold, J.D.; Cheng, X.; Hansen, C. Effects of current velocity on the nascent architecture of stream microbial biofilms. *Appl. Environ. Microbiol.* **2003**, *69*, 5443–5452.
46. Picioreanu, C.; Loosdrecht, M.C.M. van; Heijnen, J.J. A theoretical study on the effect of surface roughness on mass transport and transformation in biofilms. *Biotechnol. Bioeng.* **2000**, *68*, 355–369.
47. Picioreanu, C.; Loosdrecht, M.C.M.V.; Heijnen, J.J. Effect of diffusive and convective substrate transport on biofilm structure formation: A two-dimensional modeling study. *Biotechnol. Bioeng.* **2000**, *69*, 504–515.
48. Alpkvist, E.; Picioreanu, C.; Loosdrecht, M.C.M. van; Heyden, A. Three-dimensional biofilm model with individual cells and continuum EPS matrix. *Biotechnol. Bioeng.* **2006**, *94*, 961–979.
49. Freires, I.A.; Bueno-Silva, B.; Galvão, L.C. de C.; Duarte, M.C.T.; Sartoratto, A.; Figueira, G.M.; Alencar, S.M. de; Rosalen, P.L. The effect of essential oils and bioactive fractions on *Streptococcus mutans* and *Candida*

albicans biofilms: A confocal analysis available online: https://www.hindawi.com/journals/ecam/2015/871316/ (accessed on Feb 11, 2019).

50. Rodriguez, D.; Einarsson, B.; Carpio, A. Biofilm growth on rugose surfaces. *Phys. Rev. E* **2012**, *86*, 061914.
51. Wagner, M.; Ivleva, N.P.; Haisch, C.; Niessner, R.; Horn, H. Combined use of confocal laser scanning microscopy (CLSM) and Raman microscopy (RM): Investigations on EPS – Matrix. *Water Res.* **2009**, *43*, 63–76.
52. Fang, F.; Lu, W.-T.; Shan, Q.; Cao, J.-S. Characteristics of extracellular polymeric substances of phototrophic biofilms at different aquatic habitats. *Carbohydr. Polym.* **2014**, *106*, 1–6.
53. Polizzi, B.; Bernard, O.; Ribot, M. A time-space model for the growth of microalgae biofilms for biofuel production. *J. Theor. Biol.* **2017**, *432*, 55–79.